HHS Public Access

Author manuscript

Clin Pharmacol Ther. Author manuscript; available in PMC 2019 November 01.

Published in final edited form as:

Clin Pharmacol Ther. 2019 November ; 106(5): 1056–1066. doi:10.1002/cpt.1506.

PET Imaging of [^{11}C]Rosuvastatin Hepatic Concentrations and Hepatobiliary Transport in Humans in the Absence and Presence of Cyclosporine A

Sarah Billington[1,*], **Steven Shoner**[2], **Scott Lee**[3], **Kindra Clark-Snustad**[3], **Matthew Pennington**[4], **David Lewis**[2], **Mark Muzi**[2], **Shirley Rene**[2], **Jean Lee**[2], **Tot Bui Nguyen**[1], **Vineet Kumar**[1], **Kazuya Ishida**[1,#], **Laigo Chen**[5], **Xiaoyan Chu**[6], **Yurong Lai**[7], **Laurent Salphati**[8], **Cornelis E. C. A. Hop**[8], **Guangqing Xiao**[9], **Mingxiang Liao**[10], **Jashvant D. Unadkat**[1]

[1]Department of Pharmaceutics, University of Washington, Seattle, Washington, USA.

[2]Department of Radiology, University of Washington, Seattle, Washington, USA.

[3]Inflammatory Bowel Disease Program, University of Washington, Seattle, Washington, USA.

[4]Department of Anesthesiology & Pain Medicine, University of Washington, Seattle Washington, USA.

[5]Early Clinical Development, Worldwide Research and Development, Pfizer Inc., Cambridge, Massachusetts, USA.

[6]Pharmacokinetics, Pharmacodynamics and Drug Metabolism, Merck & Co., Kenilworth, New Jersey, USA.

[7]Department of Drug Metabolism, Gilead Sciences, Inc., Foster City, California, USA.

[8]Drug Metabolism and Pharmacokinetics, Genentech, Inc., South San Francisco, California, USA.

[9]Drug Metabolism and pharmacokinetics, Biogen, Cambridge, Massachusetts, USA. Current affiliation: Department of Drug Metabolism and Pharmacokinetics, Takeda Pharmaceuticals International Co., Cambridge, Massachusetts, USA.

Corresponding author: Jashvant D. Unadkat, jash@u.washington.edu, Department of Pharmaceutics, Box 357610, University of Washington, Seattle, WA 98195, Tel: (206) 685-2869, Fax: (206) 543-3204.

AUTHOR CONTRIBUTIONS

S.B., S.S., S.L., K.S.C., M.P., D.L., M.M., S.R., J.L., T.B.N., V.K., K.I., L.C., X.C., Y.L., L.S., C.E.C.A.H., G.X., M.L., and J.D.U. wrote the manuscript; S.B., S.S., S.L., K.S.C., M.P., D.L., M.M., S.R., T.B.N., K.I., and J.D.U. designed the research; S.B., S.S., S.L., M.P., K.S.C., D.L., S.R., J.L., V.K., T.B.N., and J.D.U. performed the research; S.B., S.R., T.B.N., and J.D.U. analyzed the data.

[*]Current affiliation: Drug Metabolism and Pharmacokinetics, Vertex Pharmaceuticals (Europe) Ltd., Abingdon-on-Thames, UK.

[#]Current affiliation: Pharmacokinetics and Drug Metabolism, Amgen, Cambridge, Massachusetts, USA.

CONFLICT OF INTEREST:

The authors declared no competing interests for this work.

SUPPLEMENTAL MATERIAL

(Supplementary Material)

Supplementary Material: Figure S1–S3, Table S1

[10]Department of Drug Metabolism and Pharmacokinetics, Takeda Pharmaceuticals International Co., Cambridge, Massachusetts, USA. Current affiliation: Clovis Oncology, San Francisco, California, USA.

Abstract

Using positron emission tomography (PET) imaging, we determined the hepatic concentrations and hepatobiliary transport of [^{11}C]rosuvastatin (IV injection) in the absence (n=6) and presence (n=4 of 6) of cyclosporine A (CsA, IV infusion) following a therapeutic dose of unlabeled rosuvastatin (RSV) (5 mg, PO) in healthy human volunteers. The sinusoidal uptake, sinusoidal efflux and biliary efflux clearance (mL/min) of [^{11}C]rosuvastatin, estimated through compartment modeling were 1205.6±384.8, 16.2±11.2 and 5.1±1.8, respectively (n=6). CsA (blood concentration: 2.77±0.24 μM), an organic-anion-transporting polypeptide (OATP), Na^+-taurocholate cotransporting polypeptide (NTCP) and breast cancer resistance protein (BCRP) inhibitor increased [^{11}C]rosuvastatin systemic blood exposure (45%; $p<0.05$), reduced its biliary efflux clearance (52%; $p<0.05$) and hepatic uptake (25%; $p>0.05$) but didn't affect its distribution into the kidneys. CsA increased plasma concentrations of coproporphyrin I and III and total bilirubin by 297±69%, 384±102% and 81±39%, respectively ($p<0.05$). These data can be used in the future to verify predictions of hepatic concentrations and hepatobiliary transport of rosuvastatin.

Keywords

Transporters; PET Imaging; In-Vitro In-Vivo Correlation; Drug-Drug Interactions; Distribution; Liver; Statins

INTRODUCTION

Success in drug approval significantly decreased from 11.2 to 5.2% between 2005–2013 (1). The main causes were lack of efficacy (~57%) and safety (~24%) of the candidate drugs (2). One contributing factor to this lack of efficacy and safety for drugs that are transported is our inability to routinely quantify (or predict) tissue concentration at the site of efficacy/toxicity. While imaging techniques such as positron emission tomography (PET) can be used to determine tissue concentrations of drugs in humans (3–5); these techniques are too costly and time-consuming for routine application during drug development (6). Therefore, there is an urgent need to develop methods to predict tissue concentration of drugs when transporters are present at the tissue: blood barrier, such as the interface between the liver, kidney, intestine, brain and blood (7).

One approach to predict drug concentration in tissues is to characterize the influx and efflux clearance (CL) of the drug of interest in primary cells derived from these tissues. However, except for hepatocytes, primary cells from other tissues (e.g. blood-brain barrier, kidney epithelial proximal tubule cells) are either not routinely available or validated. Moreover, even where available (e.g. hepatocytes), they may not be predictive of the *in-vivo* CL of the drug of interest (8–10). The reason for this lack of prediction isn't well known but could be that the abundance and/or activity of the transporters in the cells may not represent that *in-*

vivo (9). While the relative activity factor (RAF) approach can be used to surmount this shortcoming, it requires that *in-vivo* data on tissue CL (influx and efflux) be available for the probe substrate (11). Often such data are not available. In addition, as we have delineated, the systemic plasma CL of a drug is a complex function of the influx and efflux CL of drugs (12). Therefore, even if systemic CL is predicted, it cannot, by itself, be used to predict the tissue concentrations of a drug.

To address the shortcomings of the above approaches, our laboratory has hypothesized that drug concentration in tissues can be predicted from *in-vitro* CL studies in cells that individually express the transporters of interest. Then, these CL values can be scaled to that *in-vivo* (IVIVE) using the proteomics-informed bottom-up approach (9). However, such predictions must be verified to determine their accuracy. This cannot be done for every drug under development. Therefore, we propose here that such verification be conducted for selected "probe" substrates that interrogate the major transporters present in the tissue of interest. We have shown the proof-of-principle of this approach by successfully predicting the hepatic concentrations of rosuvastatin (RSV) in the rat (obtained by PET imaging (4)) by predicting the sinusoidal influx (organic-anion-transporting polypeptide (OATP)-mediated) and sinusoidal efflux CL and biliary efflux CL of RSV in cells expressing the relevant transporters (9). As a first step towards replicating this proof-of-principle in humans, we conducted for the first time [^{11}C]RSV PET imaging in humans. The primary goal was to determine the [^{11}C]RSV sinusoidal uptake CL ($CL_{s,uptake}$; mediated by OATPs and Na^+-taurocholate cotransporting polypeptide (NTCP) (13, 14)), sinusoidal efflux CL ($CL_{s,efflux}$; likely mediated by multidrug resistance-associated protein (MRP)¾ (15, 16)), biliary CL (CL_{bile}; likely mediated by breast cancer resistance protein (BCRP) (17)), as well as liver concentrations of [^{11}C]RSV (administered IV injection) following a therapeutic (PO) dose of unlabeled RSV. Our secondary goals were: i) to determine the magnitude of inhibition of the sinusoidal influx and sinusoidal/biliary efflux of RSV by an OATP/NTCP and BCRP inhibitor, cyclosporine A (CsA, administered IV infusion); and ii) to determine if the plasma biomarkers of OATP inhibition, namely coproporphyrin isomers I and III (CPI and CPIII) and total and direct bilirubin (TBILI and DBILI), are responsive to OATP inhibition by CsA.

RESULTS

Six healthy human volunteers were studied (see Table S1 for demographics) but two subjects didn't complete the CsA arm of the study either due to a delay in the first [^{11}C]RSV synthesis or an anaphylactic reaction to the CsA formulation. All subjects had haematological and chemistry values within the normal range. Except for nausea (n=3), no other side effects were reported by the subjects.

Non-compartmental analyses (NCA):

After injection, the majority of [^{11}C]RSV was rapidly distributed into the liver/gallbladder and kidneys with very little present in the rest of the body. For example, in the absence of CsA, at 30 min after [^{11}C]RSV dosing, 51.02, 2.88, 2.59 and 1.22% of the injected dose was present in the liver, gallbladder, kidneys and blood respectively with very little radioactivity present in the rest of the body (data not shown). The arterial blood and plasma area under the

concentration-time curve ($AUC_{0–30min}$) was significantly increased in the presence of CsA (Table 1, Fig. 1). The calculated mean blood-to-plasma partition ratio (BPP) was 0.64±0.06. CsA slightly reduced the distribution of [^{11}C]RSV into the liver, as measured by the maximum drug concentration in the liver (C_{max}), liver $AU_{0–30min}$ and liver-to-blood [^{11}C]RSV $AUC_{0–30min}$ ratio (Fig 1–2, Table 1). The radioactivity in the small and large intestines was equivalent to background (0–30 min), therefore, all the radioactivity in the gallbladder represented the cumulative biliary excretion of [^{11}C]RSV over 0–30min (gallbladder A_{30min}). Both gallbladder A_{30min} and biliary CL (gallbladder A_{30min}/liver $AUC_{0–30min}$) were significantly decreased by CsA (Fig. 1–2, Table 1). [^{11}C]RSV distribution into kidneys (C_{max}, time of maximal kidney drug concentration (T_{max}), and $AUC_{0–30min}$ and kidney-to-blood $AUC_{0–30min}$ ratio) was on average not significantly affected by CsA (Table 1). In the total body scans, the concentrations [^{11}C]RSV radioactivity in the brain and muscle were equivalent to background.

Compartmental analyses (CA):

$CL_{s,uptake}$ was reduced in the presence of CsA (Table 1, Fig. 3A), but this difference was found not to be statistically significant, likely due to one subject which didn't show a decrease in the presence of CsA. $CL_{s,efflux}$ was not significantly different in the presence of CsA (Table 1, Fig. 3B). CsA significantly reduced CL_{bile} of [^{11}C]RSV radioactivity (Table 1, Fig. 3C). The hepatic plasma CL (CL_h) of RSV (calculated using Eq. 4) in the absence and presence of CsA was estimated to be 25.03±5.41 L/hr and 21.22±4.27 L/hr (Fig. 3D). The confidence in the estimation of $CL_{s,uptake}$ and CL_{bile} was higher (%CV: 0.9–18.5%; Table 1) than in the estimation of $CL_{s,efflux}$ (%CV: 6.1–42.7 except for subject #1, where the %CV was 669%).

For each subject, the CsA blood concentrations during imaging were relatively constant with a mean±SD of 2.77±0.24 μM (range: 2.50–3.04 μM, %CV: <12%; Fig. S1). The plasma concentrations of unlabeled RSV in the absence of CsA (5.59±1.96 nM, n=6) were in the range of clinically observed concentrations (18). Plasma concentrations of the unlabeled RSV-lactone were below the lower limit of quantification (<4 nM).

CsA significantly increased the plasma concentrations of CPI, CPIII and TBILI (Fig. 4A–C) but not of DBILI (Fig. 4D). The largest percent change was in plasma CPIII concentrations (384±102%), followed by CPI (297±69%), TBILI (80.5±39.4%), and DBILI (75.0±50.0%). As expected, oral administration of RSV didn't affect the plasma concentrations of CPI, CPIII, TBILI or DBILI (Fig. 4A–D).

DISCUSSION

The primary goal of this human PET imaging study was to obtain estimates of hepatobiliary CL and hepatic concentrations of [^{11}C]RSV in healthy human volunteers. Once these values are available, future studies can determine if these values can be predicted by IVIVE, such as the proteomics-informed bottom-up approach. Thus, a power analysis, prior to the conduct of the study, was unnecessary. The effect of CsA on $CL_{s,uptake}$, $CL_{s,efflux}$ and hepatic concentrations of [C]RSV was secondary and therefore the study was not powered for this goal.

We deliberately chose [^{11}C]RSV to study because it has many features that make it an ideal probe for the above purpose. First, RSV is transported into the liver by OATP1B1, 1B3, 2B1 and NTCP, located on the sinusoidal membrane of hepatocytes. Second, RSV is recommended by the FDA as a clinical probe substrate for OATP1B and BCRP (19). Third, it is mostly eliminated from the body by excretion of the unchanged drug into the bile by the hepatic canalicular transporter BCRP and possibly MRP2/P-glycoprotein (P-gp) (20). Several other PET tracers have been developed to investigate hepatic transporters such as [^{11}C]telmisartan, 15-R-[^{11}C]TIC-Me, [^{11}C]dehydropravastatin, [^{11}C]glyburide, [^{11}C]erlotinib, [^{11}C]cholylsarcosine and [^{11}C]metformin (21). However, the transporters involved in the hepatic clearance of many of these compounds are either are not known or involve only a single transporter, and other tracers undergo extensive metabolism confounding interpretation of the data.

We also deliberately incorporated the following elements in our study design (Fig. 5). First, a therapeutic dose of unlabeled RSV was administered orally, on average 160±78 min (range: 65–293 min), prior to the first IV administration of [^{11}C]RSV to ensure that pharmacokinetics of [^{11}C]RSV were reflective of that of a therapeutic RSV dose (Fig. 1). Second, to prevent emptying of the gallbladder during imaging, morphine (0.04 mg/kg, IV) was given immediately prior to each IV dose of [^{11}C]RSV. Morphine causes contraction of the sphincter of Oddi (22, 23) and is a substrate of organic cation transporter (OCT) 1 (24), but its ability to be transported by or inhibit OATPs, NTCP, or BCRP has not been determined. Third, we measured plasma concentrations of [^{11}C]RSV-lactone and [^{11}C]polar metabolites in real-time by solid phase extraction (SPE) to confirm that [^{11}C]metabolites were not confounding our interpretation of plasma or tissue [^{11}C]radioactivity concentrations. Fourth, the tissue distribution of [^{11}C]RSV was studied in the absence and presence of CsA. CsA was administered as an IV infusion about 45 min prior to the 2nd IV dose of [^{11}C]RSV to allow blood CsA concentrations to reach relatively constant concentrations (Fig. S1) when dynamic images were obtained after the 2nd dose of [^{11}C]RSV as we have done before with CsA-[^{11}C]verapamil P-gp based drug-drug interaction (DDI) (3, 5, 25). CsA was chosen because at its clinically relevant plasma concentrations, in addition to OATPs, it is an inhibitor of NTCP (IC_{50}:0.37μM (14)) but rifampin (RIF) is not (IC_{50}:277 M (26)). Fifth, since OATP1B1 and BCRP are polymorphic transporters, only subjects who were not carriers of the reduced function genotypes were enrolled in the study. Sixth, after dynamic imaging (0–30 min), we conducted a head-to-thigh body scan of each subject to determine if CsA affected the distribution of [^{11}C]RSV into tissues other than the liver, gallbladder and the kidneys (e.g. muscles, the site of myotoxicity of statins). Seventh, since the impact of CsA on the more sensitive (plasma CPI, CPIII) and less sensitive OATP1B biomarkers (TBILI and TBILI) has never been studied in humans, we determined this impact.

We analysed our [^{11}C]RSV blood and tissue radioactivity data using both a noncompartmental (NCA) and compartmental (CA) approach. For CA, we used the hepatic blood [^{11}C]RSV concentration (calculated using Eq. 3) as a forcing function to obviate the need to model the disposition of [^{11}C]RSV in the blood compartment. A limitation of our study design was that we were unable to identify the hepatic artery and portal vein in the CT scans to estimate image-based input function. Therefore, peripheral arterial and venous

[^{11}C]RSV blood concentrations were used as surrogates. Our use of the peripheral venous concentration to represent portal vein concentration is reasonable unless there is significant extraction of the drug by the splanchnic bed. We assumed that such extraction was minimal given that [^{11}C]RSV was administered IV (and not orally). Distinguishing tissue concentrations of [^{11}C]RSV and [^{11}C]RSV metabolites is not possible, therefore plasma concentrations were measured as a surrogate. During the imaging period, the presence of [^{11}C]RSV-lactone in the plasma was negligible (Figure S2C). Therefore, in our NCA and CA, we assumed that the blood and tissue radioactivity measured was entirely due to [^{11}C]RSV. Use of plasma as a surrogate of liver metabolite concentration was deemed suitable, as it has been previously shown that RSV-lactone can permeate across the sinusoidal membrane (27, 28).

CsA increased (~45%) the [^{11}C]RSV blood $AUC_{0–30min}$ (Table 1) and based on the extended CL model, this suggests that CsA decreased either the $CL_{s,uptake}$ or the CL_{bile} of [^{11}C]RSV or both. Indeed CsA decreased CL_{bile} by ~52%. However if this was the only cause for the increase in [^{11}C]RSV blood AUC0–30min, because RSV is transported into the liver by OATPs/NTCP, the liver AUC0–30min should increase rather than decrease in the presence of CsA (12). On the contrary, the liver $AUC_{0–30min}$ slightly decreased indicating that CsA likely inhibited $CL_{s,uptake}$ of [^{11}C]RSV as well. This conclusion was supported by our CA of the data, where we observed that CsA inhibited $CL_{s,uptake}$ in 3 of the 4 subjects by 35–48% (Fig 3B) but didn't do so in one subject, resulting in no significant change when the data were analysed using a paired t-test. The effect of CsA on $CL_{s,uptake}$ was significant ($p<0.01$) if this subject is excluded. The changes in plasma concentrations of CPI, CPIII and TBILI were also lowest in this subject, despite blood CsA concentrations being the highest. On average CsA didn't affect $CL_{s,efflux}$, though it showed a dramatic increase in two subjects and a modest decrease in the other two. The reason for this is not known but such increase in $CL_{s,efflux}$ has been observed with other OATP substrates (29, 30). CL_h (in the absence of CsA; see Eq. 4) was 25.03±5.41 L/hr (range 14.65–30.17 L/hr), which is similar to the previously published value (35.3 L/h; total plasma clearance (48.9 L/h) – renal plasma clearance (13.6 L/h) (31).

Uptake studies in transfected cells and hepatocytes show that OATP1B1 and NTCP are the major contributors (~49 and ~35% respectively) and OATP1B3 and OATP2B1 are lesser contributors (~16% and ~0% respectively) to the total sinusoidal RSV uptake (13, 14). Efflux studies in transfected cell lines and membrane vesicles have shown that RSV is a substrate of the biliary efflux transporters BCRP, P-gp and MRP2 (17) and sinusoidal efflux transporters MRP3 and MRP4 (15, 16).

Pre-incubation can potentiate the inhibitory effect of CsA on OATP1B1 (32), therefore, in our study CsA IV infusion was designed to begin 45 min prior to [^{11}C]RSV injection. The reported concentration of CsA required to reduce uptake CL by half (IC_{50}) for the two major $CL_{s,uptake}$ transporters of RSV are 0.21 (OATP1B1) and 0.37 μM (NTCP) (14, 33). Therefore, it was not surprising that an unbound blood CsA concentration of 0.28 μM (34) caused only a 45% reduction in liver distribution of [^{11}C]RSV (Fig. 1, 6, Table 1) and increased CPI, CPIII, and TBILI plasma concentrations (Fig. 4A–C). The 45% increase in systemic [^{11}C]RSV exposure is lower than the RSVRIF (RSV: PO; RIF: 600mg, IV) DDI

studies (230%; (26)). This difference could be because we administered [^{11}C]RSV IV while in the RSV-RIF study, RSV was administered orally. Therefore, in the RSV-RIF study, RIF likely affected the first-pass hepatic extraction of RSV resulting in a bigger increase in RSV plasma concentration. The percent change in plasma concentrations of CPI, CPIII, TBILI and DBILI in our study are comparable to those observed in humans following RIF administration (35–37) and cynomologus monkeys after CsA administration (100 mg/kg, PO) (38). These percent changes are greater for the biomarkers than those for blood [^{11}C]RSV $AUC_{0–30\ min}$ because the biomarkers likely have greater fraction transported (f_t) via OATPs than RSV (which is a substrate of both OATPs and NTCP). This makes RSV a less sensitive indicator of inhibition of OATP1Bs after IV administration, but not necessarily after oral administration. CsA decreased CL_{bile} (Fig. 3C), suggesting that BCRP and possibly P-gp and MRP2 were inhibited (Fig. 6). Reported IC_{50} values for CsA of biliary efflux transporters of RSV range from 1.5 (P-gp) to 3.2 (BCRP) to 5.6 μM (MRP2) (39–41). These values cannot be directly compared with unbound blood CsA concentration as it is the intracellular (or canalicular membrane) concentrations of CsA (unknown) that should be used as a reference.

Renal clearance accounts for approximately 28% of RSV clearance, with ~90% of the renal clearance thought to result from transporter-mediated tubular secretion primarily by organic anion transporter (OAT) 3 uptake followed by apical secretion primarily by MRP2/4, BCRP and P-gp (31, 42). However, CsA, didn't affect the net renal distribution of [^{11}C]RSV indicating that it didn't inhibit the above transporters at the blood concentrations achieved (IC_{50} data are not available). Parenthetically, please note Fig. 1E shows a change in the kidney exposure in the presence of CsA but that is driven by changes in blood radioactivity; therefore the kidney-to-blood $AUC_{0–30min}$ ratio was unchanged. This conclusion was supported by no effect of CsA on the renal CL of [^{11}C]RSV (ratio of cumulative radioactivity in the bladder at 60 min and the blood $AUC_{0–60min}$; data not shown). The distribution of [^{11}C]RSV into other organs, such as the brain and muscle, was no different from background in the absence or presence of CsA. This suggests that brain penetration of [^{11}C]RSV is limited by its relatively low LogP value and/or BCRP/P-gp. Also, as we have shown before in our [^{11}C]verpamil-CsA PET imaging DDI study, the unbound blood concentrations of CsA achieved are weak inhibitors of cerebral P-gp and therefore likely BCRP. Interestingly, CsA appears to inhibit biliary efflux of [^{11}C]RSV, likely by BCRP. These observations suggest that unbound hepatic CsA concentrations are higher than those in the blood.

In conclusion, we measured for the first time the hepatic concentrations and hepatobiliary transport of [^{11}C]RSV in humans using PET imaging. In the future, these data can be used by us and others to determine if the hepatobiliary clearance of a drug can be predicted from *in-vitro* data using the proteomics-informed bottom-up approach. Furthermore, we recommend that the validity of the proposed proteomics-informed IVIVE approach be tested with additional PET imaging substrates that interrogate these and other major human hepatic and renal transporters.

METHODS

Synthesis of [^{11}C]RSV

[^{11}C]RSV was synthesized by bubbling [^{11}C]methyl-triflate ([^{11}C]CH_3OTf) into 1.0 mg desmethylrosuvastatin dissolved in dimethylsulfoxide (50μL) and acetone (50μL) (43). The product, [^{11}C]RSV, was purified on a semi-preparative reversed-phase C8 column (Luna C8(2), 250 × 4.6 mm 10μm) by eluting it at 40±10°C with sterile, nonpyrogenic mobile phase, 40:60 [v:v] USP ethanol:sterile, 0.1% formic acid solution (3 mL/min). The product was sterilized by filtration (0.2μm filter), diluted with USP saline (final ethanol conc. <10%; [v/v]) and pH adjusted to 7.0 with USP sodium bicarbonate and sodium phosphate. The average decay corrected reaction yield of [^{11}C]RSV was 50–70%, and the final product was 99.95±0.01% radiochemically pure, apyrogenic with a specific activity of 146.6±33.4 GBq/μmol (range: 91.4–180.0 GBq/μmol; n=10). Stability was measured out to 40 min post-synthesis with no significant degradation of the product observed.

Subjects

Six subjects with normal complete blood cell count, hepatic and renal function tests, and prothrombin time were enrolled (Table S1). Subjects who were pregnant (re-confirmed negative on study day), breast-feeding, had polymorphic SLC01B1/ABCG2 genotypes (i.e. SLCO1B1 c.521TC, c.521CC, c.1463CC; ABCG2 c.421AA), with a history of a chronic medical condition(s), on chronic medication (except oral contraceptives), smokers, or with a history of substance abuse were excluded. No medication (other than acetaminophen), caffeinated or alcoholic beverages were allowed for at least 24 hours before the study. Due to ethnic differences in disposition of statins, subjects of Chinese, Japanese, Malay, Filipino, Korean, Vietnamese or Indian ethnicity (self-reported) were excluded (27, 28). The study was approved by the University of Washington's Human Subjects IRB Review Committee, Radiation Safety Committee, and Radioactive Drug Research Committee.

SLCO1B1 and ABCG2 Genotyping

The Gentra Puregene Buccal Cell Kit from Qiagen (Germantown, MD) was used to extract genomic DNA from buccal swabs according to the manufacturer's protocol. Polymorphisms in SLCO1B1 (c.388G>A, c.521T>C and c.1463G>C) and ABCG2 (c.421C>A) were determined using validated Applied Biosystems TaqMan SNP Genotyping Assays from Applied Biosystems (Foster City, CA).

PET-CT Scans

To minimize emptying of the gallbladder, subjects fasted (except water) from 4 hours prior to RSV dosing to study completion. On arrival at the PET imaging suite, the subjects were equipped with an antecubital venous catheter in each arm (one for [^{11}C]RSV/morphine administration/CsA infusion and the other for venous blood sampling) and an arterial catheter (radial artery; for arterial blood sampling). After collecting a venous blood sample, subjects received a 5 mg RSV tablet (Crestor®) orally. All unlabeled drugs, including RSV, were supplied by the UWMC Pharmacy. PET scans were acquired on a GE Discovery STE PET/CT scanner (GE Medical, Waukesha, WI) using a low-dose CT transmission scan for

attenuation correction (resolution (mm): 4.29 in-plane, 3.27 axial). The study sequence and details are provided in Fig. 5.

Blood sampling and analysis

Arterial (5 of 6 subjects) and venous (4 of 6 subject) blood samples were collected at various time-points to measure concentrations of [^{11}C]radioactivity, RSV, RSV-lactone, CPI, CPIII, TBILI and DBILI in blood and/or plasma (Fig. 5). To measure blood and plasma radioactivity, aliquots of blood (200 μL) and plasma (200 μL; isolated immediately after blood collection) were counted using a gamma counter (Cobra Counter; Packard, Meridian, CT). Assessment of the [^{11}C]RSV radioactivity arterial-venous blood concentration ratio revealed that they differed until 4 min (Fig. S2A–B). Therefore, for subjects that had arterial but not venous blood sampled, the arterial-venous concentration ratio was used to estimate venous blood concentrations, and vice-versa. In the measurement of plasma unlabeled RSV and RSV-lactone concentrations, 0.3M sodium acetate buffer (NaOAc; pH 4.0) was immediately added to plasma (1:1) to stabilise rosuvastatin-lactone before LCMS/MS analysis with minor modification of an assay published previously (44). Blood concentrations of CsA and plasma concentrations of DBILI/TBILI were measured by LC-MS/MS and spectrophotometry, respectively (Laboratory Medicine at UWMC). Plasma concentrations of CPI and CPIII were quantified by LC-MS/MS with minor modification of an assay published previously (35, 38).

Quantification of plasma [^{11}C]RSV and [^{11}C]metabolite concentrations

Immediately after isolation, each plasma sample was combined with 0.3M sodium acetate (NaOAc) buffer solution [pH 4.0] containing unlabeled RSV and RSV-lactone (10 μg/mL) (1:1 [v:v]) and loaded onto a BondElut C_{18} SPE cartridge (size: 500 mg/3cc; Varian, Inc, Lake Forest, Calif) and eluted as follows with a manual pressure pump: (1) 0.1M NaOAc buffer [pH 4.0] (6 mL) (2) 0.1M NaOAc buffer: acetonitrile (ACN) (75:25 [v:v]); 10 mL) (3) 0.1M NaOAc buffer: ACN (65:35 [v:v]; 0.5 mL) (4) 0.1M NaOAc buffer: ACN (55:45 [v:v]; 2 mL), and (5) 0.1M NaOAc buffer: ACN (30:70 [v:v]; 1.5 mL). Validation studies showed that RSV and RSV-lactone eluted only in the 55:45 and 30:70 NaOAc buffer:ACN fractions [v:v], respectively. The 100% NaOAc buffer fraction contained polar metabolites. The recovery of the unlabeled RSV and RSV-lactone in individual fractions, diluted 5-fold in 0.1M NaOAc buffer: ACN (40:60 [v:v]), determined by HPLC/UV, was found to be 96.1±5.9 % and 96.4±10.0 %, respectively. HPLC/UV conditions were: $C_{18,}$ BetaBasic column (150 × 2.1 mm, 5 μm); gradient mobile phase consisting of (A) aqueous 0.05% formic acid and (B) acetonitrile (15% B hold for 1 min, 15–25% B 1–3 min, 25–40% B 3–18 min, 40–46% B, 18–30 min, 46–95% B 30–31 min, hold 95% for 2 min; flow rate: 300 μL/min; UV detection at 244 nm). With the use of these recovery values, the radioactive content of each fraction was corrected and expressed as a fraction of that contained in the unextracted plasma sample. Plasma concentrations of [^{11}C]rosuvastatin lactone and [^{11}C]polar-metabolites was negligible up to 45 min (Figure S2C), therefore, blood, plasma and tissue radioactivity was attributed to [^{11}C]RSV.

Analysis of PET Imaging Data

PET images were reconstructed using a 3D reconstruction algorithm (iterative logarithm with 6 subsets and 28 iterations) with correction for scattered and random coincidences. The tomograph, dose calibrator, and gamma counter were cross-calibrated to express all measurements in common units of radioactivity (kBq/cc). Regions of interest (ROIs) were drawn manually across all image planes for the liver, left kidney, gallbladder, and the small and large intestines using PMOD (v.3.5;PMOD Technologies LLC, Zürich, Switzerland). The ROIs from contiguous slices were combined to create volumes of interest (VOIs) for each tissue. The regions were drawn away from vascular bundles, bile ducts and borders of the organs to minimise organ-boundary edge artefacts and were viewed in coronal, sagittal, and axial directions to ensure that different VOIs didn't overlap. CT images were used for secondary confirmation of the anatomic accuracy of the PET VOIs. VOIs were applied to both the dynamic image sets and the static summed standardized uptake value (SUV) images for data extraction. Radioactivity in the gallbladder was assumed to correspond to radioactivity excreted into bile and data analysis was confined to 0–30 min.

Non-compartmental Analysis of [^{11}C]RSV Radioactivity Data

Time-radioactivity curves for arterial blood and tissues were constructed from decay-corrected time radioactivity measurements. Tissue and arterial blood AUC were estimated by the trapezoidal rule. CL_{bile} was calculated by gallbladder $A_{,30}/AUC_{liver,0–30}$. Gallbladder $A_{,30}$, the cumulative amount of radioactivity in the gallbladder at 30 min, is the radioactivity concentration in the gallbladder at 30 min (kBq/cc) multiplied by the (weight-adjusted) fasted gallbladder volume.

Compartmental Analysis of [^{11}C]RSV Radioactivity Data

A two compartment model (Fig. 3F, Eq. 1 and 2) was fitted, using SAAM II and the relative data-weighting scheme, to the [^{11}C]RSV liver and gallbladder radioactivity concentration-versus-time data.

$$\frac{dA_L}{dt} = CL_{s,uptake} \cdot C_B - \left(CL_{s,efflux} + CL_{bile}\right) \cdot C_L \quad \text{(Equation 1)}$$

$$\frac{dA_{GB}}{dt} = CL_{bile} \cdot C_L \quad \text{(Equation 2)}$$

Where A, C, B, L, GB, $CL_{s,uptake}$, $CL_{s,efflux}$, CL_{bile} represent amount, concentration, blood, liver, gallbladder, sinusoidal uptake clearance, sinusoidal efflux clearance and biliary efflux clearance, respectively. Since the portal vein and hepatic artery contribute 80% and 20% of the total liver blood supply (45), the hepatic input blood concentrations of [^{11}C]RSV (C_B) (used as the forcing function in the model (Fig. 1)), were estimated using equation 3. C_{venous} and $C_{arterial}$ represent the radioactivity concentrations in peripheral arterial and venous blood samples.

$$C_B = C_{Venous} \cdot 0.8 + C_{Arterial} \cdot 0.2 \quad \text{(Equation 3)}$$

The volume of blood, liver, gallbladder and the volume of blood within the liver were fixed to weight adjusted physiological values (46). Lag times from blood to liver (~0.3 min) and liver to gallbladder (~3.1 min) were incorporated into the model based on visual inspection of the data. Goodness of fit of the model to the data was evaluated by visual inspection, confidence in the estimates of the parameters, weighted residual plots and Q-Q plots. The fit of the model to data for all subjects can be seen in Figure S3.

Estimation of Plasma Hepatic Clearance

The extended CL model (47) can be used to estimate plasma CL_h (Eq. 4) using our estimates of $CL_{s,uptake}$, $CL_{s,efflux}$, CL_{bile}, BPP) and values of hepatic blood flow (Q_h;1500 mL/min) and hepatic metabolic clearance of RSV (CL_{met}). Note, CL_{met} referred to here is that based on the unbound hepatic RSV concentration. For this reason, we do not have an estimate of CL_{met} nor is it available in the literature. Literature data supports the notion that hepatic uptake is the rate-determining step in the hepatic clearance of the drug (48–50). Therefore, assuming that hepatic uptake is the rate-determining step, we estimated RSV CL_h using Eq. 4, where $f_{u.b} \cdot CL_{\text{intrinsic uptake}}$ is equal to $CL_{s,uptake}$.

$$CL_h = \frac{Q_h \cdot f_{u,b} \cdot CL_{\text{intrinsic uptake}}}{Q_h + f_{u.b} \cdot CL_{\text{intrinsic uptake}}} \cdot BPP \quad \text{(Equation 4)}$$

Statistical Analysis

Statistical difference in pharmacokinetic parameters was determined by both a paired t-test (n=4) and unpaired t-test (see Table 1).

Supplementary Material

Refer to Web version on PubMed Central for supplementary material.

ACKNOWLEDGMENTS

We thank Madhav Sachar, Lena Anoshchenko, Neha Maharo and technicians at UWMC PET-CT suite for their assistance during the study. We thank Christy Callahan, Elisa Beebe, Caitlin Kerwin and colleagues at UW for their help in IRB submission and subject screening. We thank Rena Zhang, Gaungping Bi, Joan Ellis and Ken Anderson (of Merck) for their bioanalytical support.

FUNDING

This work was supported by UWRAPT through funding from Biogen, Genentech, Gilead Sciences, Merck, Pfizer and Takeda.

REFERENCES

1. Wong CH, Siah KW, Lo AW. Corrigendum: Estimation of clinical trial success rates and related parameters. Biostatistics. 2018.

2. Harrison RK. Phase II and phase III failures: 2013–2015 Nat Rev Drug Discov. 15 England2016 p. 817–8. [PubMed: 27811931]

3. Sasongko L, Link JM, Muzi M, Mankoff DA, Yang X, Collier AC, et al. Imaging P-glycoprotein transport activity at the human blood-brain barrier with positron emission tomography. Clin Pharmacol Ther. 2005;77(6):503–14. [PubMed: 15961982]

4. He J, Yu Y, Prasad B, Link J, Miyaoka RS, Chen X, et al. PET imaging of Oatp-mediated hepatobiliary transport of [(11)C] rosuvastatin in the rat. Mol Pharm. 2014;11(8):2745–54. [PubMed: 24957348]

5. Eyal S, Ke B, Muzi M, Link JM, Mankoff DA, Collier AC, et al. Regional P-glycoprotein activity and inhibition at the human blood-brain barrier as imaged by positron emission tomography. Clin Pharmacol Ther. 2010;87(5):579–85. [PubMed: 20336065]

6. Guo Y, Chu X, Parrott NJ, Brouwer KLR, Hsu V, Nagar S, et al. Advancing Predictions of Tissue and Intracellular Drug Concentrations Using In Vitro, Imaging and Physiologically Based Pharmacokinetic Modeling Approaches. Clin Pharmacol Ther. 2018;104(5):865–89. [PubMed: 30059145]

7. Endres CJ, Hsiao P, Chung FS, Unadkat JD. The role of transporters in drug interactions. Eur J Pharm Sci. 2006;27(5):501–17. [PubMed: 16364611]

8. Jones HM, Barton HA, Lai Y, Bi YA, Kimoto E, Kempshall S, et al. Mechanistic pharmacokinetic modeling for the prediction of transporter-mediated disposition in humans from sandwich culture human hepatocyte data. Drug Metab Dispos. 2012;40(5):1007–17. [PubMed: 22344703]

9. Ishida K, Ullah M, Toth B, Juhasz V, Unadkat JD. Successful Prediction of In Vivo Hepatobiliary Clearances and Hepatic Concentrations of Rosuvastatin Using Sandwich-Cultured Rat Hepatocytes, Transporter-Expressing Cell Lines, and Quantitative Proteomics. Drug Metab Dispos. 2018;46(1): 66–74. [PubMed: 29084782]

10. De Bruyn T, Ufuk A, Cantrill C, Kosa RE, Bi YA, Niosi M, et al. Predicting Human Clearance of Organic Anion Transporting Polypeptide Substrates Using Cynomolgus Monkey: In Vitro-In Vivo Scaling of Hepatic Uptake Clearance. Drug Metab Dispos. 2018;46(7):989–1000. [PubMed: 29720472]

11. Chapy H, Klieber S, Brun P, Gerbal-Chaloin S, Boulenc X, Nicolas O. PBPK modeling of irbesartan: incorporation of hepatic uptake. Biopharm Drug Dispos. 2015;36(8):491–506. [PubMed: 26037524]

12. Patilea-Vrana G, Unadkat JD. Transport vs. Metabolism: What Determines the Pharmacokinetics and Pharmacodynamics of Drugs? Insights From the Extended Clearance Model. Clin Pharmacol Ther. 2016;100(5):413–8. [PubMed: 27448198]

13. Kitamura S, Maeda K, Wang Y, Sugiyama Y. Involvement of multiple transporters in the hepatobiliary transport of rosuvastatin. Drug Metab Dispos. 2008;36(10):2014–23. [PubMed: 18617601]

14. Ho RH, Tirona RG, Leake BF, Glaeser H, Lee W, Lemke CJ, et al. Drug and bile acid transporters in rosuvastatin hepatic uptake: function, expression, and pharmacogenetics. Gastroenterology. 2006;130(6):1793–806. [PubMed: 16697742]

15. Pfeifer ND, Yang K, Brouwer KL. Hepatic basolateral efflux contributes significantly to rosuvastatin disposition I: characterization of basolateral versus biliary clearance using a novel protocol in sandwich-cultured hepatocytes. J Pharmacol Exp Ther. 2013;347(3):727–36. [PubMed: 24023367]

16. Kanda K, Takahashi R, Yoshikado T, Sugiyama Y. Total hepatocellular disposition profiling of rosuvastatin and pitavastatin in sandwich-cultured human hepatocytes. Drug Metab Pharmacokinet. 2018;33(3):164–72. [PubMed: 29724614]

17. Ieiri I, Higuchi S, Sugiyama Y. Genetic polymorphisms of uptake (OATP1B1, 1B3) and efflux (MRP2, BCRP) transporters: implications for inter-individual differences in the pharmacokinetics and pharmacodynamics of statins and other clinically relevant drugs. Expert Opin Drug Metab Toxicol. 2009;5(7):703–29. [PubMed: 19442037]

18. Martin PD, Warwick MJ, Dane AL, Cantarini MV. A double-blind, randomized, incomplete crossover trial to assess the dose proportionality of rosuvastatin in healthy volunteers. Clin Ther. 2003;25(8):2215–24. [PubMed: 14512129]

19. Giacomini KM, Huang SM, Tweedie DJ, Benet LZ, Brouwer KL, Chu X, et al. Membrane transporters in drug development. Nat Rev Drug Discov. 2010;9(3):215–36. [PubMed: 20190787]
20. Martin PD, Warwick MJ, Dane AL, Hill SJ, Giles PB, Phillips PJ, et al. Metabolism, excretion, and pharmacokinetics of rosuvastatin in healthy adult male volunteers. Clin Ther. 2003;25(11):2822–35. [PubMed: 14693307]
21. Tournier N, Stieger B, Langer O. Imaging techniques to study drug transporter function in vivo. Pharmacol Ther. 2018;189:104–22. [PubMed: 29684469]
22. Helm JF, Venu RP, Geenen JE, Hogan WJ, Dodds WJ, Toouli J, et al. Effects of morphine on the human sphincter of Oddi. Gut. 1988;29(10):1402–7. [PubMed: 3197985]
23. Krishnamurthy S, Krishnamurthy GT. Cholecystokinin and morphine pharmacological intervention during 99mTc-HIDA cholescintigraphy: a rational approach. Semin Nucl Med. 1996;26(1):16–24. [PubMed: 8623048]
24. Tzvetkov MV, dos Santos Pereira JN, Meineke I, Saadatmand AR, Stingl JC, Brockmoller J. Morphine is a substrate of the organic cation transporter OCT1 and polymorphisms in OCT1 gene affect morphine pharmacokinetics after codeine administration. Biochem Pharmacol. 2013;86(5):666–78. [PubMed: 23835420]
25. Muzi M, Mankoff DA, Link JM, Shoner S, Collier AC, Sasongko L, et al. Imaging of cyclosporine inhibition of P-glycoprotein activity using 11C-verapamil in the brain: studies of healthy humans. J Nucl Med. 2009;50(8):1267–75. [PubMed: 19617341]
26. Prueksaritanont T, Chu X, Evers R, Klopfer SO, Caro L, Kothare PA, et al. Pitavastatin is a more sensitive and selective organic anion-transporting polypeptide 1B clinical probe than rosuvastatin. Br J Clin Pharmacol. 2014;78(3):587–98. [PubMed: 24617605]
27. Lee E, Ryan S, Birmingham B, Zalikowski J, March R, Ambrose H, et al. Rosuvastatin pharmacokinetics and pharmacogenetics in white and Asian subjects residing in the same environment. Clin Pharmacol Ther. 2005;78(4):330–41. [PubMed: 16198652]
28. Birmingham BK, Bujac SR, Elsby R, Azumaya CT, Zalikowski J, Chen Y, et al. Rosuvastatin pharmacokinetics and pharmacogenetics in Caucasian and Asian subjects residing in the United States. Eur J Clin Pharmacol. 2015;71(3):329–40. [PubMed: 25630984]
29. Pfeifer ND, Goss SL, Swift B, Ghibellini G, Ivanovic M, Heizer WD, et al. Effect of Ritonavir on (99m)Technetium-Mebrofenin Disposition in Humans: A Semi-PBPK Modeling and In Vitro Approach to Predict Transporter-Mediated DDIs. CPT Pharmacometrics Syst Pharmacol. 2013;2:e20. [PubMed: 23887590]
30. Bauer M, Matsuda A, Wulkersdorfer B, Philippe C, Traxl A, Ozvegy-Laczka C, et al. Influence of OATPs on Hepatic Disposition of Erlotinib Measured With Positron Emission Tomography. Clin Pharmacol Ther. 2018;104(1):139–47. [PubMed: 28940241]
31. Martin PD, Warwick MJ, Dane AL, Brindley C, Short T. Absolute oral bioavailability of rosuvastatin in healthy white adult male volunteers. Clin Ther. 2003;25(10):2553–63. [PubMed: 14667956]
32. Izumi S, Nozaki Y, Maeda K, Komori T, Takenaka O, Kusuhara H, et al. Investigation of the impact of substrate selection on in vitro organic anion transporting polypeptide 1B1 inhibition profiles for the prediction of drug-drug interactions. Drug Metab Dispos. 2015;43(2):235–47. [PubMed: 25414411]
33. Shen H, Su H, Liu T, Yao M, Mintier G, Li L, et al. Evaluation of rosuvastatin as an organic anion transporting polypeptide (OATP) probe substrate: in vitro transport and in vivo disposition in cynomolgus monkeys. J Pharmacol Exp Ther. 2015;353(2):380–91. [PubMed: 25740896]
34. Zaghloul I, Ptachcinski RJ, Burckart GJ, Van Thiel D, Starzel TE, Venkataramanan R. Blood protein binding of cyclosporine in transplant patients. J Clin Pharmacol. 1987;27(3):240–2. [PubMed: 3316307]
35. Lai Y, Mandlekar S, Shen H, Holenarsipur VK, Langish R, Rajanna P, et al. Coproporphyrins in Plasma and Urine Can Be Appropriate Clinical Biomarkers to Recapitulate Drug-Drug Interactions Mediated by Organic Anion Transporting Polypeptide Inhibition. J Pharmacol Exp Ther. 2016;358(3):397–404. [PubMed: 27317801]
36. Shen H, Chen W, Drexler DM, Mandlekar S, Holenarsipur VK, Shields EE, et al. Comparative Evaluation of Plasma Bile Acids, Dehydroepiandrosterone Sulfate, Hexadecanedioate, and

Tetradecanedioate with Coproporphyrins I and III as Markers of OATP Inhibition in Healthy Subjects. Drug Metab Dispos. 2017;45(8):908–19. [PubMed: 28576766]

37. Chu X, Liao M, Shen H, Yoshida K, Zur AA, Arya V, et al. Clinical Probes and Endogenous Biomarkers as Substrates for Transporter Drug-Drug Interaction Evaluation: Perspectives From the International Transporter Consortium. Clin Pharmacol Ther. 2018;104(5):836–64. [PubMed: 30347454]
38. Shen H, Dai J, Liu T, Cheng Y, Chen W, Freeden C, et al. Coproporphyrins I and III as Functional Markers of OATP1B Activity: In Vitro and In Vivo Evaluation in Preclinical Species. J Pharmacol Exp Ther. 2016;357(2):382–93. [PubMed: 26907622]
39. Rautio J, Humphreys JE, Webster LO, Balakrishnan A, Keogh JP, Kunta JR, et al. In vitro pglycoprotein inhibition assays for assessment of clinical drug interaction potential of new drug candidates: a recommendation for probe substrates. Drug Metab Dispos. 2006;34(5):786–92. [PubMed: 16455806]
40. Lechner C, Reichel V, Moenning U, Reichel A, Fricker G. Development of a fluorescence-based assay for drug interactions with human Multidrug Resistance Related Protein (MRP2; ABCC2) in MDCKII-MRP2 membrane vesicles. Eur J Pharm Biopharm. 2010;75(2):284–90. [PubMed: 20307659]
41. Miyata H, Takada T, Toyoda Y, Matsuo H, Ichida K, Suzuki H. Identification of Febuxostat as a New Strong ABCG2 Inhibitor: Potential Applications and Risks in Clinical Situations. Front Pharmacol. 2016;7:518. [PubMed: 28082903]
42. Verhulst A, Sayer R, De Broe ME, D'Haese PC, Brown CD. Human proximal tubular epithelium actively secretes but does not retain rosuvastatin. Mol Pharmacol. 2008;74(4):1084–91. [PubMed: 18612079]
43. Link JM, Krohn KA, Clark JC. Production of [11C]CH3I by single pass reaction of [11C]CH4 with I2. Nucl Med Biol. 1997;24(1):93–7. [PubMed: 9080480]
44. Chu X, Shih SJ, Shaw R, Hentze H, Chan GH, Owens K, et al. Evaluation of cynomolgus monkeys for the identification of endogenous biomarkers for hepatic transporter inhibition and as a translatable model to predict pharmacokinetic interactions with statins in humans. Drug Metab Dispos. 2015;43(6):851–63. [PubMed: 25813937]
45. Schenk WG Jr., Mc DJ, Mc DK, Drapanas T. Direct measurement of hepatic blood flow in surgical patients: with related observations on hepatic flow dynamics in experimental animals. Ann Surg. 1962;156:463–71. [PubMed: 14498225]
46. Mattsson S, Johansson L, Leide Svegborn S, Liniecki J, Nosske D, Riklund KA, et al. Radiation Dose to Patients from Radiopharmaceuticals: a Compendium of Current Information Related to Frequently Used Substances Ann ICRP. 44 England2015 p. 7–321.
47. Endres CJ, Endres MG, Unadkat JD. Interplay of drug metabolism and transport: a real phenomenon or an artifact of the site of measurement? Mol Pharm. 2009;6(6):1756–65. [PubMed: 19886641]
48. Cooper KJ, Martin PD, Dane AL, Warwick MJ, Schneck DW, Cantarini MV. The effect of fluconazole on the pharmacokinetics of rosuvastatin. Eur J Clin Pharmacol. 2002;58(8):527–31. [PubMed: 12451430]
49. Pasanen MK, Fredrikson H, Neuvonen PJ, Niemi M. Different effects of SLCO1B1 polymorphism on the pharmacokinetics of atorvastatin and rosuvastatin. Clin Pharmacol Ther. 2007;82(6):726–33. [PubMed: 17473846]
50. Bailey KM, Romaine SP, Jackson BM, Farrin AJ, Efthymiou M, Barth JH, et al. Hepatic metabolism and transporter gene variants enhance response to rosuvastatin in patients with acute myocardial infarction: the GEOSTAT-1 Study. Circ Cardiovasc Genet. 2010;3(3):276–85. [PubMed: 20207952]

STUDY HIGHLIGHTS

What is the current knowledge on the topic?

Currently, measurement or prediction of tissue concentrations of drugs is not routinely possible. We have developed a proteomics-informed approach to predict tissue concentrations of drugs.

What question did this study address?

Through positron emission tomography (PET) imaging, for the first time, we measured the hepatic concentrations and hepatobiliary clearances of a model organic-anion-transporting polypeptide (OATP) and breast cancer resistance protein (BCRP) substrate, [^{11}C]rosuvastatin in humans.

What does this study add to our knowledge?

Hepatobiliary clearance of [^{11}C]rosuvastatin appears to be rate-determined by its sinusoidal uptake clearance and hepatic blood flow. Cyclosporine A, an inhibitor of multiple transporters, reduced the biliary efflux and likely sinusoidal uptake clearance of [^{11}C]rosuvastatin.

How might this change clinical pharmacology or translational science?

These data can be used to verify proteomics-informed prediction of transporter-mediated tissue drug concentrations and disposition in humans. Once verified, this approach can be routinely applied to predict tissue drug concentrations during drug development.

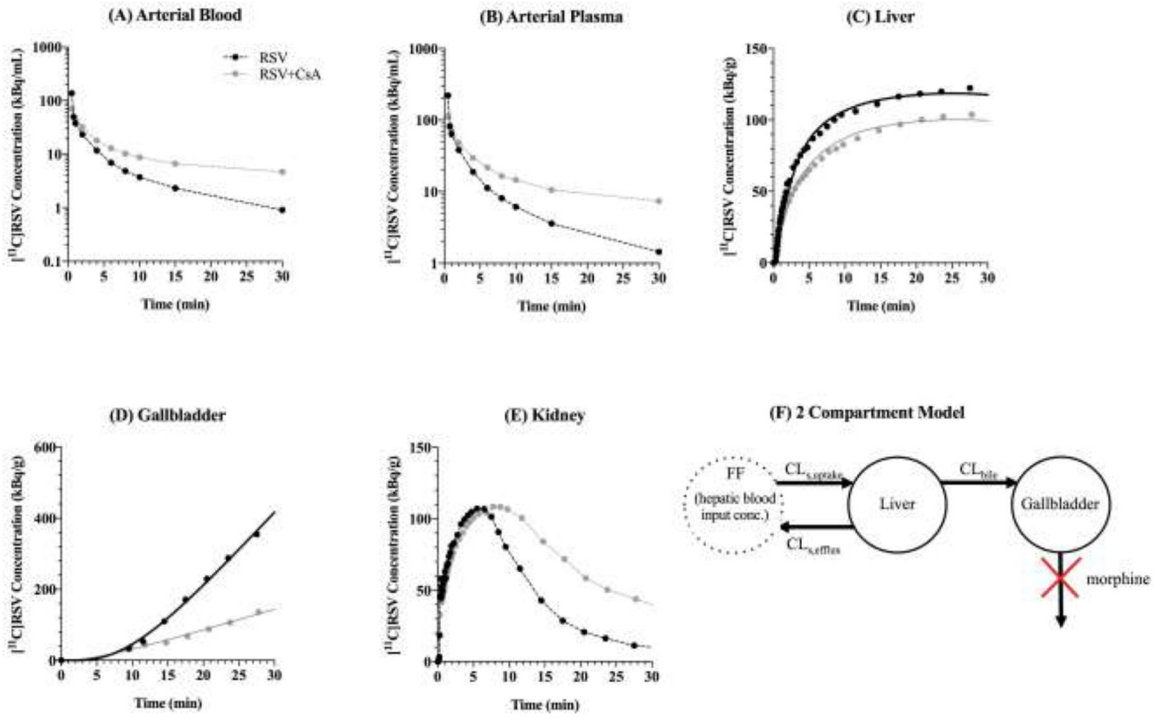

Figure 1:

Radioactivity concentration-versus-time profiles in the arterial blood (A), arterial plasma (B), liver (C), gallbladder (D), and kidney (E) in a representative subject in the absence and presence of cyclosporine A (CsA). CsA caused an increase in blood and plasma [^{11}C]rosuvastatin (RSV) concentrations and reduction in liver and gallbladder concentrations of [^{11}C]RSV. (F) The two-compartment pharmacokinetic model used to fit the liver and gallbladder [^{11}C]RSV radioactivity-versus-time profiles in the absence and presence of CsA. Estimated hepatic input blood concentrations of [^{11}C]RSV (Eq. 3) were used as the forcing function (FF). Solid lines represent the model fit to the liver and gallbladder concentrations.

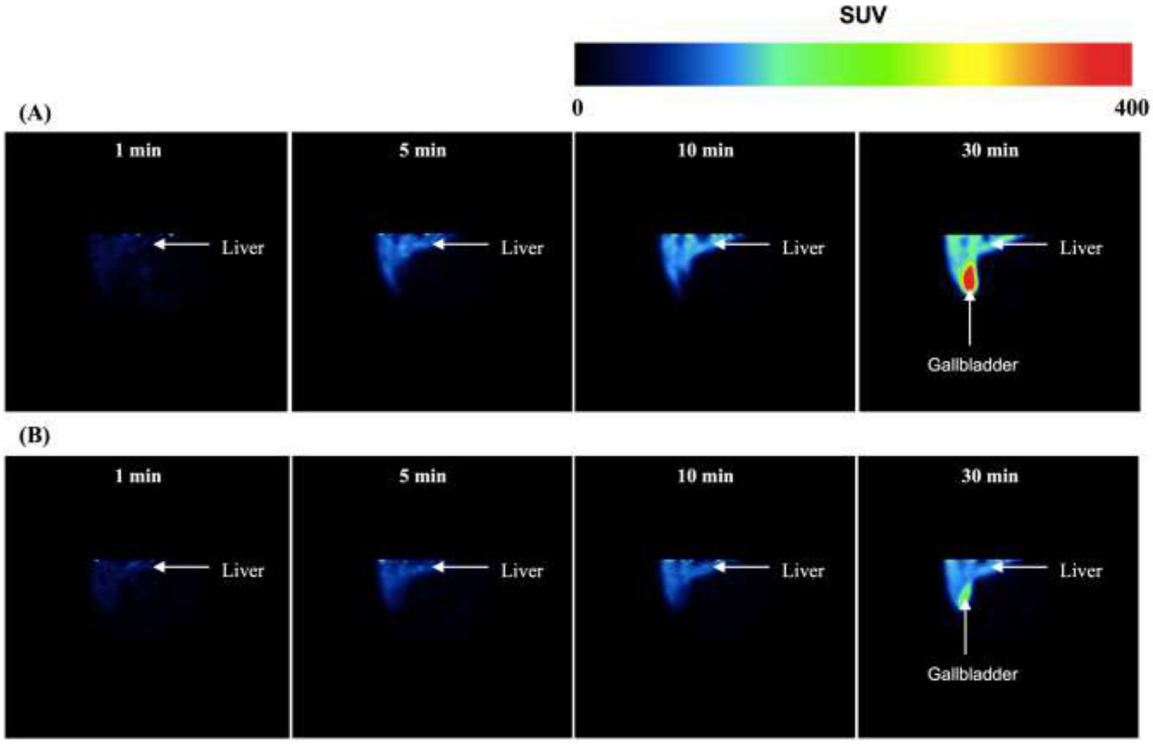

Figure 2:

Representative coronal standard uptake value (SUV; tissue radioactivity, KBq/g)/(injected radioactivity, KBq x body mass, g)) images of a normal human liver and gallbladder after [^{11}C]rosuvastatin (RSV) administration in the absence (A) and presence (B) of cyclosporine A (CsA). CsA reduced the uptake of [^{11}C]RSV into the liver and decreased the efflux of [^{11}C]RSV into the gallbladder.

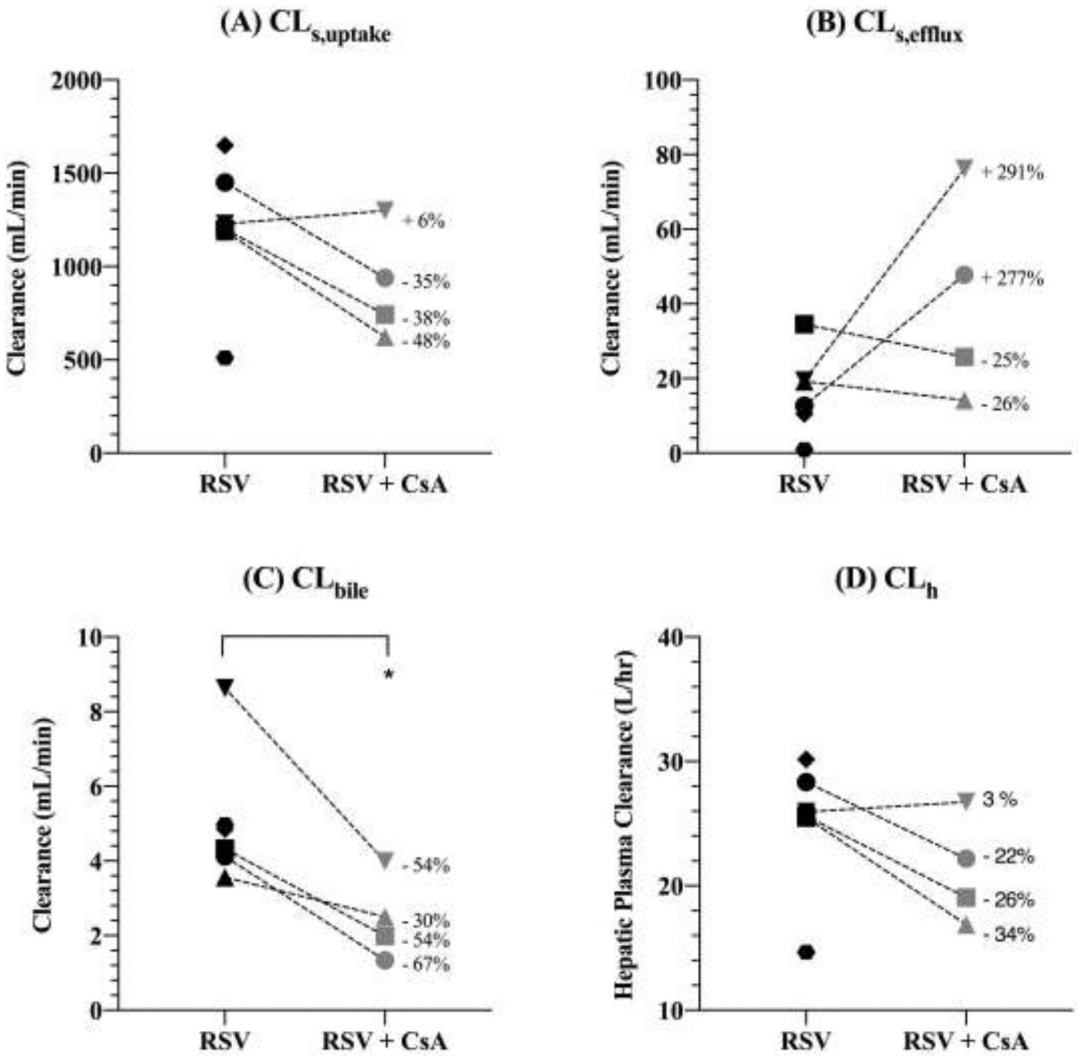

Figure 3:

Estimates of [^{11}C]rousvastatin (RSV) sinusoidal uptake clearance ($CL_{s,uptake}$; A), sinusoidal efflux clearance ($CL_{s,efflux}$; B), biliary efflux clearance (CL_{bile}; C) and hepatic plasma clearance (CL_h; D) in the absence and presence of cyclosporine A (CsA) obtained by compartmental modeling. CL_h was estimated using the hepatic well-stirred model (Eq. 4). CsA caused a significant decrease in CL_{bile}. $CL_{s,uptake}$, $CL_{s,efflux}$ and CL_h were not significantly affected by CsA, though CsA did reduce $CL_{s,uptake}$ and CL_h in 3 of the 4 subjects. Statistical significance was determined by the paired t-test. Each symbol represents the same individual in each panel, * indicates $p<0.05$. The percent change in the value of each parameter in the presence of CsA is shown.

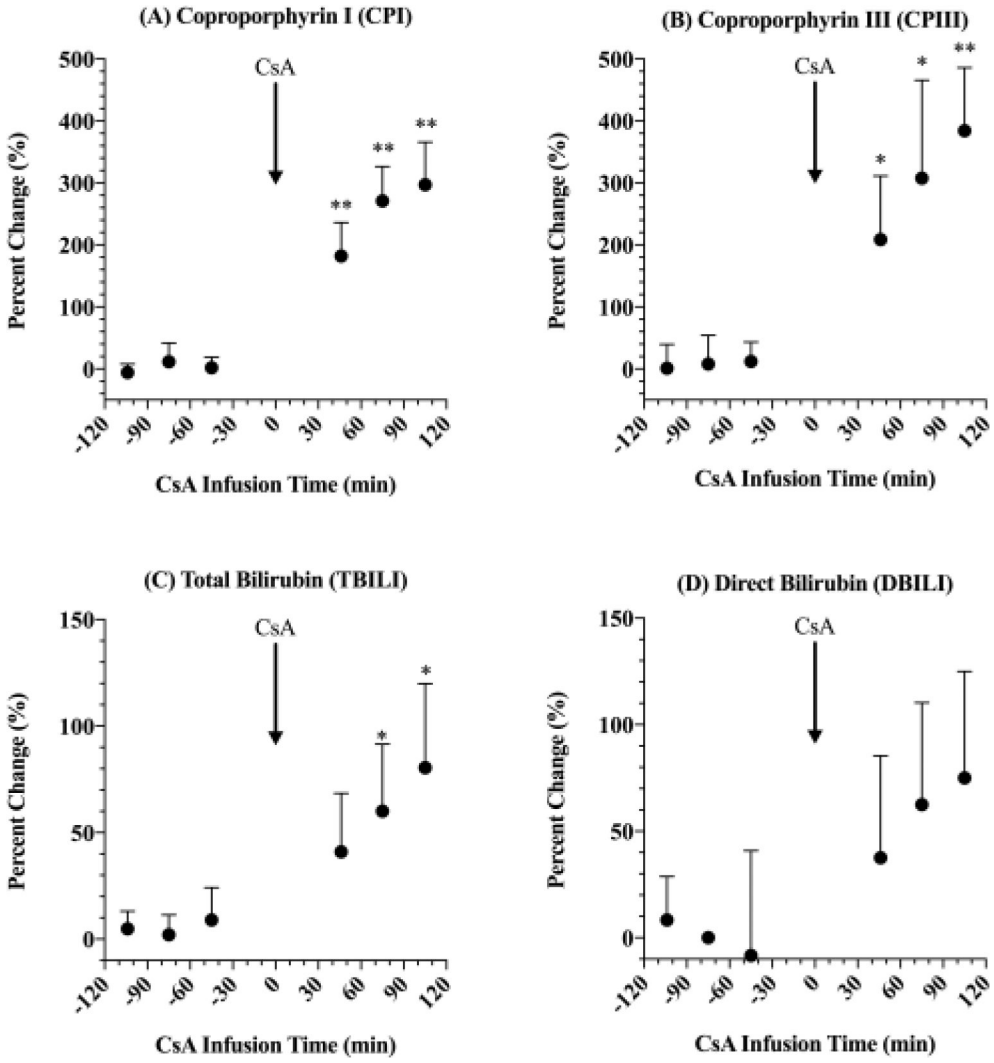

Figure 4:

The percent change in plasma concentrations of coproporphyrin (CP) I (A) and III (B), total bilirubin (TBILI; C) and direct bilirubin (DBILI; D) in the presence of rosuvastatin (RSV) and cyclosporine A (CsA). Data normalized to plasma concentration of endogenous biomarkers before administration of RSV. CsA (in combination with RSV) caused a significant increase in plasma concentrations of CPI, CPIII and TBILI. RSV alone (−120 to 0 min) didn't affect plasma concentrations of endogenous biomarkers. Statistical significance was determined by a one-sample t-test, * and ** indicate $p<0.05$ and $p<0.01$, respectively.

(A)

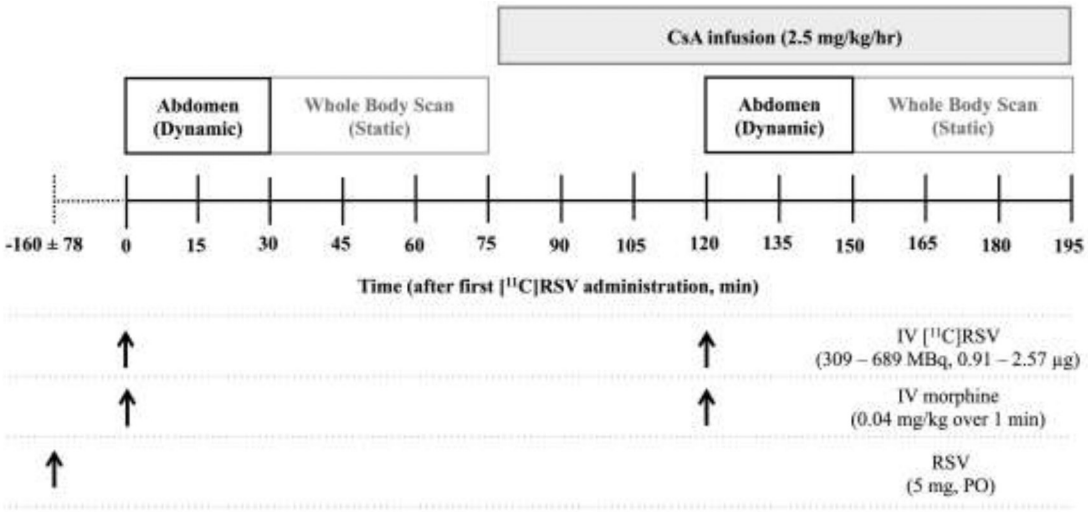

(B)

Measurement	Sampling time-points (time post-[11C]RSV injection, min)
Arterial blood & plasma [11C]radioactivity concentration	0.5, 0.75, 1, 2, 4, 6, 8, 10, 15, 30, 45, 60
Venous blood [11C]radioactivity concentration	0.5, 0.75, 1, 2, 4, 6, 8, 10, 15, 30
Plasma [11C]RSV & [11C]metabolite concentration	0.5, 0.75, 1, 2, 4, 6, 8, 10, 15, 30, 45
Unlabeled plasma RSV & RSV-lactone concentration	0.5, 0.75, 1, 2, 4, 6, 8, 10, 15, 30, 45, 60
Plasma coproporphyrin I & III concentration	Baseline* , 1, 30, 60
Plasma total bilirubin and direct bilirubin concentration	Baseline* , 1, 30, 60
	(time post-CsA infusion start, min)
Blood CsA concentration	15, 30, 45, 60, 90, 120

Footnotes: **A blood sample was collected before PO administration of RSV to measure baseline plasma concentrations of coproporphyrin I & III, total bilirubin and direct bilirubin.*

Figure 5:

Timeline for administration of the [11C]rosuvastatin (RSV; IV injection), cyclosporine A (CsA; IV infusion), morphine (IV injection) and RSV (PO) to assess hepatic concentrations and hepatobiliary transport of [11C]RSV in the absence and presence of CsA (A). A 5 mg dose of RSV (PO) was given 160±78 min prior to PET imaging to ensure that [11C]RSV pharmacokinetics was comparable to that when clinical doses of RSV are given. Morphine was given immediately prior to each dose [11C]RSV to prevent emptying of the gallbladder. Dynamic images of the liver and gallbladder were taken over 30 min to measure the hepatic concentrations and hepatobiliary clearance of [11C]RSV. Dynamic images of the kidneys were taken over 30 min to measure the renal concentrations and renal clearance of [11C]RSV. A scan of the body, from head to mid-thigh, was performed after dynamic imaging of the abdomen, to measure liver, gallbladder, intestinal, kidney, brain and muscle concentrations of [11C]RSV. Blood samples were taken to match the imaging sequence to measure concentrations of [11C]radioactivity, unlabeled RSV and RSV-lactone, CsA, coproporphyrin I and III, total and direct bilirubin (B).

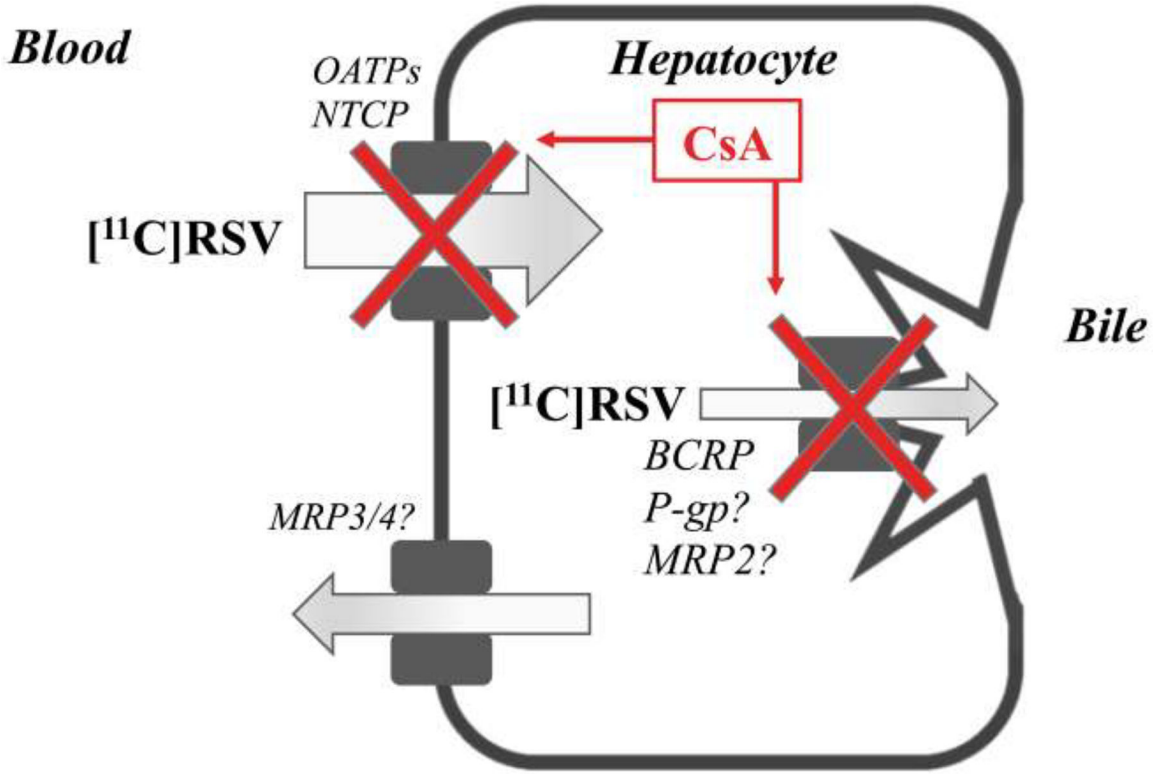

Figure 6:

Proposed mechanism of the transporter-mediated drug-drug interaction between [^{11}C]rosuvastatin (RSV) and cyclosporine A (CsA). CsA significantly reduced the distribution of [^{11}C]RSV into the liver via inhibition of organic-anion-transporting polypeptide (OATP)1B-mediated sinusoidal uptake ($CL_{s,uptake}$) of [^{11}C]RSV, as evidenced by the increase in plasma concentrations of coproporphyrin I and III and total bilirubin. Na^+-taurocholate cotransporting polypeptide (NTCP)-mediated uptake may also be partially inhibited based upon published IC_{50} values (the concentration of CsA required to reduce NTCP-mediated uptake CL by half). CsA significantly reduced the biliary clearance (CL_{bile}) of [^{11}C]RSV by inhibition of breast cancer resistance protein (BCRP), and possibly p-glycoprotein (P-gp)/multidrug resistance protein (MRP)2. CsA didn't affect the sinusoidal efflux clearance ($CL_{s,efflux}$) of [^{11}C]RSV possibly mediated by MRP3/MRP4.

Clin Pharmacol Ther. Author manuscript; available in PMC 2019 November 01.

Table 1:

Non-compartmental and compartmental estimation of hepatobiliary disposition of [^{11}C]RSV in humans when administered alone or in the presence of CsA.

Non-Compartmental Data Analysis	**RSV (n=6)**		**RSV + CsA (n=4)**		**Percent Change**	**P-value (paired t-test)**	**P-value (unpaired t-test)**
	Mean	**SD**	**Mean**	**SD**			
Blood C_{max} (Bq/mL/kBq)	0.24	0.07	0.22	0.09	−8.3%	ns	ns
Blood T_{max} (min)	1.53	0.79	1.37	0.80	−10.5%	ns	ns
Blood $AUC_{0–30mm}$ (min*Bq/mL/kBq)	0.67	0.11	0.97	0.20	44.8%	*	*
Plasma C_{max} (Bq/mL/kBq)	0.38	0.11	0.35	0.12	−7.9%	ns	ns
Plasma $AUC_{0–30min}$ (min*Bq/mL/kBq)	1.06	0.14	1.54	0.24	45.3%	*	*
Liver T_{max} (min)	25.90	2.20	27.00	1.30	4.2%	ns	ns
Liver C_{max} (Bq/g/kBq)	0.32	0.10	0.28	0.05	−12.5%	*	ns
Liver $AUC_{0–30min}$ (min*Bq/g/kBq)	8.07	2.62	6.75	1.27	−16.4%	*	ns
Liver $AUC_{0–30min}$ / Blood $AUC_{0–30min}$	12.66	5.83	6.97	0.77	−44.9%	*	ns
Gallbladder A_{30min} (Bq/kBq)	28.61	8.29	10.45	2.42	−63.5%	*	*
Gallbladder A_{30min} / Liver $AUC_{0–30min}$ (mL/min)	3.83	1.75	1.62	0.62	−57.7%	*	*
Kidney T_{max} (min)	7.30	1.90	7.20	0.60	−1.4%	ns	ns
Kidney C_{max} (Bq/g/kBq)	0.35	0.08	0.41	0.15	17.1%	ns	ns
Kidney $AUC_{0–30min}$ (min*Bq/g/kBq)	5.83	2.56	5.87	2.07	0.7%	ns	ns
Kidney $AUC_{0–30min}$ / Blood $AUC_{0–30min}$	8.80	4.02	6.34	2.80	−28.0%	ns	ns
Compartmental Data Analysis	**RSV (n=6)**		**RSV + CsA (n=4)**		**Percent Change**	**P-value (paired t-test)**	**P-value (unpaired t-test)**
	Mean	**SD**	**Mean**	**SD**			
$CL_{s,uptake}$ (mL/min)	1205.6	384.8	900.7	295.6	−25.29%	ns	ns
$CL_{s,efflux}$ (mL/min)	16.24	11.24	41.00	27.31	152.46%	ns	ns
CL_{bile} (mL/min)	5.08	1.81	2.46	1.13	−51.57%	*	*

Statistical significance was determined by both a paired t-test, comparing the 4 subjects that completed both study arms, and an unpaired t-test, comparingthe subjects as two distinct groups. This is because two of the subjects did not complete the CsA arm of the study.

* indicates $p<0.05$.